Article

Synthesis and Characterization of Potent Bivalent Amyloidosis Inhibitors That Bind Prior to Transthyretin Tetramerization

Nora S. Green, Satheesh K. Palaninathan, James C. Sacchettini, and Jeffery W. Kelly

J. Am. Chem. Soc., **2003**, 125 (44), 13404-13414• DOI: 10.1021/ja030294z • Publication Date (Web): 01 October 2003

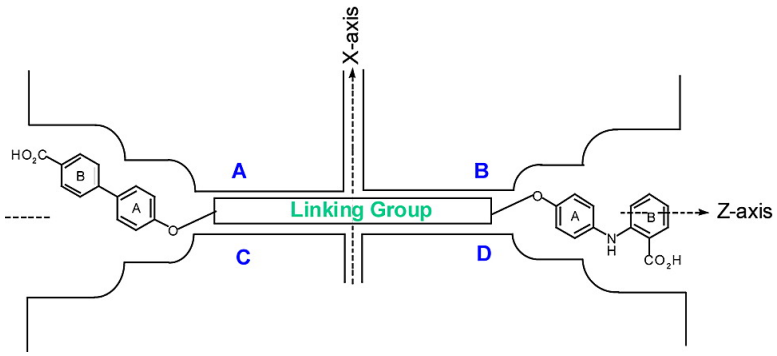

More About This Article

Additional resources and features associated with this article are available within the HTML version:

- Supporting Information
- Links to the 5 articles that cite this article, as of the time of this article download
- Access to high resolution figures
- Links to articles and content related to this article
- Copyright permission to reproduce figures and/or text from this article

View the Full Text HTML

J|A|C|S
ARTICLES
Published on Web 10/01/2003

Synthesis and Characterization of Potent Bivalent Amyloidosis Inhibitors That Bind Prior to Transthyretin Tetramerization

Nora S. Green,[†] Satheesh K. Palaninathan,[‡] James C. Sacchettini,[‡] and Jeffery W. Kelly*,[†]

Contribution from the Department of Chemistry and Skaggs Institute for Chemical Biology, The Scripps Research Institute, 10550 North Torrey Pines Road, BCC265, La Jolla, California 92037, and Department of Biochemistry and Biophysics, Texas A&M University, College Station, Texas 77843-2128

Received May 15, 2003; E-mail: jkelly@scripps.edu

Abstract: The misfolding of transthyretin (TTR), including rate-limiting tetramer dissociation and partial monomer denaturation, is sufficient for TTR misassembly into amyloid and other abnormal quaternary structures associated with senile systemic amyloidosis, familial amyloid polyneuropathy, and familial amyloid cardiomyopathy. Monovalent small molecules that bind to one or both of the unoccupied thyroid hormone binding sites at the TTR quaternary structure interface stabilize the native state, raising the kinetic barrier for tetramer dissociation sufficiently that the rate of dissociation, and therefore amyloidosis, becomes slow. Bivalent amyloid inhibitors that bind to both binding sites simultaneously are reported herein. The candidate bivalent inhibitors are generally unable to bind to the native TTR tetramer and typically do not engage in monovalent binding owing to a strong inhibitor orientation preference. However, the TTR quaternary structure can assemble around several of the bivalent inhibitors if the inhibitor intercepts the protein before assembly occurs. Some of the wild-type TTR·bivalent inhibitor complexes prepared in this fashion retain a tetrameric structure when subjected to substantial denaturation stresses (8 M urea, 120 h). The best bivalent inhibitor reduced acid-mediated TTR (3.6 μM) amyloid fibril formation to 6% of that exhibited by TTR in the absence of inhibitor, a significant improvement over the ~30% observed for the best monovalent inhibitors (3.6 μM, 72 h). The apparent dissociation rate of the best bivalent inhibitor is effectively zero, consistent with the idea that TTR tetramer dissociation and inhibitor dissociation are linked—as a result of the inhibitor-templating tetramer assembly. X-ray cocrystal structures of two of the complexes demonstrate that the bivalent inhibitors simultaneously occupy both sites in TTR, consistent with the 1:1 binding stoichiometry derived from HPLC analysis. The purpose of this study was to demonstrate that bivalent inhibitors could be useful; what resulted are the best inhibitors produced to date. In this context, molecules capable of intercepting TTR during folding and assembly in the lumen of the endoplasmic reticulum would be of obvious interest.

Introduction

Transthyretin (TTR) is a tetrameric protein comprised of identical 127 amino acid β-sheet sandwich subunits.[1] The functions of TTR are to transport holoretinol binding protein and thyroxine (T4) in the blood and CSF.[2] Under mildly acidic conditions, the tetramer dissociates and the monomers partially unfold and misassemble into amyloid fibrils and amorphous aggregates.[3] The stoichiometry of T4 bound to TTR in plasma and CSF is less than 0.05, allowing us to target these sites to prevent amyloidogenesis.[4] Deposition of full-length wild-type (WT) transthyretin in the heart and peripheral nerves putatively causes senile systemic amyloidosis (SSA),[5] whereas the deposition of one of eighty TTR variants is associated with a group of diseases collectively known as familial amyloid polyneuropathy (FAP).[6] The mutations D18G and A25T are representative of about a dozen FAP mutations that lead to central nervous system (CNS) deposition and pathology.[7] Amyloidogenesis of V122I TTR results in familial amyloid cardiomyopathy (FAC), putting 1 million African Americans at significant risk for congestive heart failure.[8]

[†] The Scripps Research Institute.
[‡] Texas A&M University.

(1) (a) Blake, C. C.; Swan, I. D.; Rerat, C.; Berthou, J.; Laurent, A.; Rearta, B. *J. Mol. Biol.* **1971**, *61*, 217−224. (b) Blake, C. C.; Geisow, M. J.; Oatley, S. J.; Rerat, B.; Rerat, C. *J. Mol. Biol.* **1978**, *121*, 339−356.
(2) (a) Monaco, H. L.; Rizzi, M.; Coda, A. *Science* **1995**, *268*, 1039−1041. (b) Nilsson, S. F.; Rack, L.; Peterson, P. *J. Biol. Chem.* **1975**, *250*, 8554−8563.
(3) (a) Colon, W.; Kelly, J. W. *Biochemistry* **1992**, *31*, 8654−8660. (b) Lai, Z.; Colon, W.; Kelly, J. W. *Biochemistry* **1996**, *35*, 6470−6482. (c) Kelly, J. W.; Colon, W.; Lai, Z.; Lashuel, H. A.; McCulloch, J.; McCutchen, S. L.; Milroy, G. J.; Peterson, S. A. *Adv. Protein Chem.* **1997**, *50*, 161−181. (d) Lashuel, H. A.; Lai, Z.; Kelly, J. W. *Biochemistry* **1998**, *37*, 17851−17864. (e) (b) Liu, K.; Cho, H. S.; Lashuel, H. A.; Kelly, J. W.; Wemmer, D. E. *Nat. Struct. Biol.* **2000**, *7*, 754−757.
(4) Bartalena, L.; Robbins, J. *Clin. Lab. Med.* **1993**, *13*, 583−598.
(5) (a) Westermark, P.; Sletten, K.; Johansson, B.; Cornwell, G. G., III. *Proc. Natl. Acad. Sci. U.S.A.* **1990**, *87*, 2843−5. (b) McCarthy, R. E., III; Kasper, E. K. *Clin. Cardiol.* **1998**, *21*, 547−552.
(6) (a) Saraiva, M. J.; Costa, P. P.; Goodman, D. S. *J. Clin. Invest.* **1985**, *76*, 2171−2177. (b) Plante-Bordenuve, V.; Said, G. *Curr. Opin. Neurol.* **2000**, *13*, 569−573.

10.1021/ja030294z CCC: $25.00

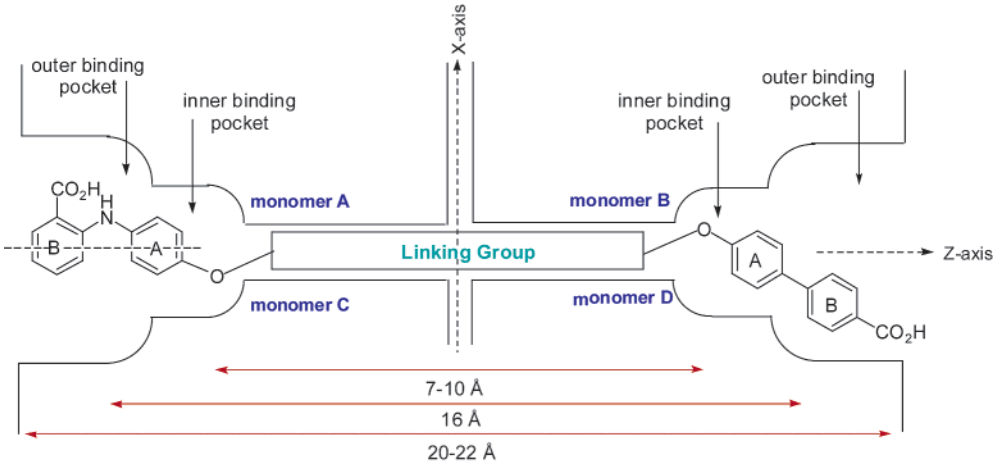

Figure 1. Schematic representation of the tetrameric structure of transthyretin. There are two symmetry-related thyroxine binding sites per tetramer. The two binding sites are connected by a central channel that runs through the TTR tetramer. Bivalent inhibitors are envisioned to bind with one substructure in each of the two thyroxine binding sites connected by a linking group that threads the channel.

The two identical funnel-shaped thyroxine binding sites located at the TTR dimer−dimer interface are interconverted by two C_2 axes oriented perpendicular to the crystallographic 2-fold axis (*z*-axis), Figure 1.[9] The two binding sites are connected by a very narrow channel centered on the *z*-axis. Using both limited screening and structure-based design, we have previously reported a large number of compounds that are capable of inhibiting TTR fibril formation by binding to the thyroxine sites.[9,10] Previous studies demonstrate that the most dramatic reduction of TTR fibril formation occurs when both T4 binding sites are occupied by inhibitors that bind with high affinity and exhibit slow dissociation rates.[11] Ligands that bind with high affinity to both sites (K_{d1} and K_{d2} < 10 nM) stabilize the TTR·inhibitor$_2$ complex to the extent that the activation energy for the rate-limiting step of amyloidogenesis (tetramer dissociation) is no longer available under most denaturing conditions, including acid-mediated amyloidogenesis conditions.[11]

A single bivalent molecule that occupies both T4 sites simultaneously could have several important advantages over traditional monovalent inhibitors, including high binding affinity and selectivity, as well as a slow dissociation rate. Most monovalent TTR amyloidosis inhibitors display negatively cooperative binding because ΔH_2 is greater than ΔH_1.[9−11] There is some evidence that when the first equivalent of these inhibitors bind, there is a change in the second TTR binding site as discerned from NMR titration experiments.[13] One can covalently link two different inhibitors, each known to have high affinity for TTR's T4 binding sites, in the search for potent bivalent inhibitors. Optimally the linker should be fairly rigid and designed to perfectly match the geometric requirements of the central channel. This minimizes the conformational entropy penalty associated with binding, allowing full advantage to be taken of the fact that $\Delta S_{trans} + \Delta S_{rot}$ only has to be paid once for a bivalent inhibitor.[12] Linkers with too much flexibility are generally problematic because $\Delta S_{conf} \geq \Delta S_{trans} + \Delta S_{rot}$; hence, the added affinity derived from only having to pay $\Delta S_{trans} + \Delta S_{rot}$ once is lost.[12] When $\Delta S_{conf} \geq \Delta S_{trans} + \Delta S_{rot}$, it is generally the case that inhibitors having the potential to bind in a bivalent fashion bind to the receptor in a monovalent fashion. Monovalent binding of a potentially bivalent inhibitor should be disfavored for the inhibitors synthesized herein because the substructures selected to occupy the T4 sites have a preferred orientation, which would need to be reversed for monovalent binding.[9,10]

Bivalent inhibitors can be administered at ca. half the dose of traditional amyloidogenesis inhibitors, minimizing toxicity caused by the unbound inhibitor. Recent examples of other approaches to bivalent inhibitors include alkyl-linked benzamidine inhibitors of human lung tryptase,[14] bistetrahydroaminacrine inhibitors of acetylcholinesterase,[15] and nonpeptide inhibitors of the matrix metalloproteinase stromelysin.[16]

There are at least three potential mechanisms that would allow bivalent inhibitors to bind both T4 binding sites simultaneously. If one of the substructures envisioned to occupy a T4 site is

(7) (a) Vidal, R.; Garzuly, F.; Budka, H.; Lalowski, M.; Linke, R. P.; Brittig, F.; Frangione, B.; Wisniewski, T. *Am. J. Pathol.* **1996**, *148*, 361−366. (b) Sekijima, Y.; Hammarstrom, P.; Matsumura, M.; Shimizu, Y.; Iwata, M.; Tokuda, T.; Ikeda, S.; Kelly, J. W. *Lab. Invest.* **2003**, *83*, 409−417. (c) Hammarstrom, P.; Sekijima, Y.; White, J. T.; Costello, C. E.; Altland, K.; Garzuly, F.; Budke, H.; Kelly, J. W. *Biochemistry* **2003**, 6656−6663.
(8) Jacobson, D. R.; Pastore, R. D.; Yaghoubian, R.; Kane, I.; Gallo, G.; Buck, F. S.; Buxbaum, J. N. *N. Engl. J. Med.* **1997**, *336*, 466−473.
(9) Sacchettini, J. C.; Kelly, J. W. *Nat. Rev. Drug Discov.* **2002**, *1*, 267−275.
(10) (a) Peterson, S. A.; Klabunde, T.; Lashuel, H. A.; Purkey, H.; Sacchettini, J. C.; Kelly, J. W. *Proc. Natl. Acad. Sci. U.S.A.* **1998**, *95*, 12956−12969. (b) Baures, P. W.; Peterson, S. A.; Kelly, J. W. *Bioorg. Med. Chem.* **1998**, *6*, 1389−1401. (c) Baures, P. W.; Oza, V. B.; Petersen, S. A.; Kelly, J. W. *Bioorg. Med. Chem.* **1999**, *7*, 1339−1347. (d) Petrassi, H. M.; Klablunde, T.; Sacchettini, J. C.; Kelly, J. W. *J. Am. Chem. Soc.* **2000**, *122*, 2178−2192. (e) Klabunde, T.; Petrassi, H. M.; Oza, V. B.; Raman, P.; Kelly, J. W. *Nat. Struct. Biol.* **2000**, *7*, 312−321. (f) Oza, V. B.; Smith, C.; Raman, P.; Koepf, E. K.; Laushel, H. A.; Petrassi, H. M.; Chiang, K. P.; Powers, E. T.; Sacchettini, J. C.; Kelly, J. W. *J. Med. Chem.* **2002**, *45*, 321−332. (g) Razavi, H.; Palaninathan, S. K.; Powers, E. T.; Wiseman, R. L.; Purkey, H. E.; MohamedMohaideen, N. N.; Deechongkit, S.; Chiang, K. P.; Dendle, M. T. A.; Sacchettini, J. C.; Kelly, J. W. *Angew. Chem., Int. Ed.*, **2003**, *42*, 2758−2761.
(11) Hammarstrom, P.; Wiseman, R. L.; Powers, E. T.; Kelly, J. W. *Science* **2003**, *299*, 713−716.
(12) Mammen, M.; Seok-Ki, C.; Whitesides, G. M. *Angew. Chem., Int. Ed.* **1998**, *37*, 2754−2794.
(13) Reid, D. G.; MacLachlan, L. K.; Voyle, M.; Leeson, P. D. *J. Biol. Chem.* **1989**, *4*, 2013−2023.
(14) Burgess, L. E.; Newhouse, B. J.; Ibraham, P.; Rizzi, J.; Kashem, M. A.; Hartman, A.; Brandhuber, B. J.; Wright, C. D.; Thomson, C. D.; Vigers, G. P. A.; Koch, K. *Proc. Natl. Acad. Sci. U.S.A.* **1999**, *96*, 8348−8352.
(15) (a) Pang, Y.-P.; Quiram, P.; Jalecic, T.; Hong, F.; Brimijoin, S. *J. Biol. Chem.* **1996**, *217*, 23646−23649. (b) Schaschke, N.; Dominik, A.; Matschiner, G.; Sommerhoff, C. P. *Bioorg. Med. Chem. Lett.* **2002**, *12*, 985−988.
(16) Hadjuk, P. J.; Sheppard, G.; Nettesheim, D. G.; Olejniczak, E. T.; Shuker, S. B.; Meadows, R. P.; Steinman, D. H.; Carrera, G. M., Jr.; Marcotte, P. A.; Severin, J.; Walter, K.; Smith, H.; Gubbins, E.; Simmer, R.; Holzman, T. F.; Morgan, D. W.; Davidsen, S. K.; Summers, J. B.; Fesik, S. W. *J. Am. Chem. Soc.* **1997**, *119*, 5818−5827.

small enough, the bivalent inhibitor could thread through the central channel of the tetramer from one end during breathing motions (the "threading mechanism"). This would require that the recognition substructure of the bivalent inhibitor transiently occupy the first encountered binding site in the nonpreferred orientation, which would be energetically unfavorable. Another possibility is that the bivalent inhibitor could bind sequentially to TTR subunits liberated from the tetramer during the subunit exchange known to occur under physiological conditions (the "subunit exchange mechanism").[17] Given that monomeric TTR folds faster than it assembles, we envision that the most efficient mechanism of bivalent inhibitor binding would involve intercepting the protein before or during quaternary structure formation (the "pre- or coassembly mechanism").[19] Tetramer assembly around the dumbbell-shaped inhibitor could lead to an exceedingly slow bivalent inhibitor dissociation rate—a characteristic of ideal amyloidosis inhibitors.[11]

Herein, bivalent inhibitor design, synthesis, efficacy, and mechanism of action are probed by a variety of experiments. Bivalent inhibitors are only able to bind to TTR by the pre- or coassembly mechanism. In fact, some of the inhibitors are capable of tetramerizing D18G, a monomer whose facile misfolding from a monomeric state leads to CNS pathology.[7] X-ray crystallographic studies demonstrate that at least two of the bivalent inhibitors bind, as envisioned, to both sites simultaneously, consistent with the 1:1 binding stoichiometry determined by HPLC.[18] The best inhibitor reduced fibril formation to 6% of that exhibited by TTR in the absence of inhibitor, significantly better than the ~30% (3.6 μM, 72 h) observed with the better monovalent inhibitors. The TTR·bivalent inhibitor complex cannot be denatured in 8.0 M urea, even after incubation for 120 h. The apparent dissociation rate of the best inhibitor is effectively zero, implying that after TTR assembles around the inhibitor neither the protein nor the inhibitor can dissociate. While the purpose of this study was to provide a proof of principle that bivalent inhibitors are viable, what resulted are the best inhibitors that we have produced to date.

Results

Design and Synthesis of Bivalent Inhibitors. Three monovalent TTR amyloidosis inhibitors (Figure 2) were selected to compose the bivalent inhibitors.[10] As monovalent binders, each displayed excellent fibril formation inhibition properties (Figure 3) at a concentration of 7.2 μM, twice the concentration of TTR subjected to amyloidosis conditions (3.6 μM). Moreover, the phenol functionality in each serves as an ideal functional group to link the three monovalent inhibitors in all combinations. Both homo- and heterobivalent compounds were synthesized for this study, employing linkers that include commercially available dihaloalkanes, ethylene glycol ditosylates, or unsaturated diols. Ideal linker lengths (Figure 1) were estimated from the X-ray crystal structure of transthyretin bound to 2 equiv of flufenamic acid.[9] The central channel connecting the two binding sites is just wide enough to accommodate an alkyl chain of the proper length and conformation.

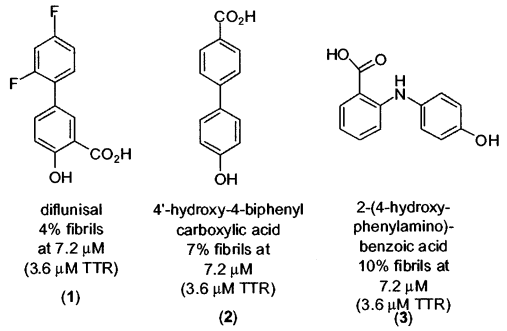

Figure 2. Monovalent TTR amyloidogenesis inhibitors whose structures are covalently linked through their phenol groups to form the bivalent inhibitors studied herein. Each exhibits excellent fibril inhibition efficacy (7.2 μM) when incubated with TTR (3.6 μM) for 72 h in the standard acid-mediated fibril formation assay (pH 4.4; see Fig 3, inset).

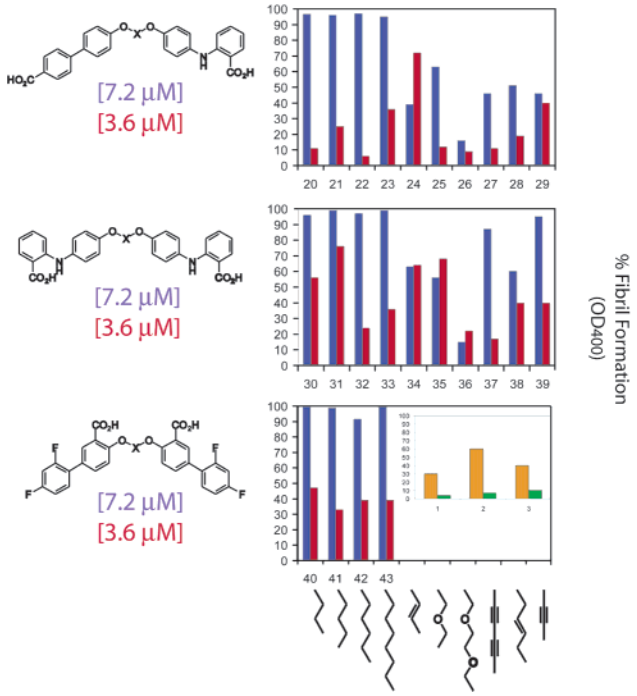

Figure 3. Extent of inhibition of acid-mediated WT TTR fibril formation by inhibitors **20**−**43**. The generic structure on the left-hand side of each bar graph can be completed by inserting the linking group **X** shown at the bottom. Blue bars represent data from a traditional fibril formation assay wherein tetrameric TTR (3.6 μM) is preincubated with inhibitor (7.2 μM) for 30 min prior to dropping the pH to 4.4 (72 h). Red bars represent acid-mediated fibril formation data from TTR·inhibitor complexes prepared by incubating the inhibitor with TTR undergoing folding and assembly (pre- or coassembly mechanism), affording TTR·bivalent inhibitor complexes of 1:1 stoichiometry. The orange and green bars of the inset depict WT TTR (3.6 μM) fibril inhibition data for the monovalent inhibitors **1**−**3** at 3.6 and 7.2 μM, respectively. The *y*-axis in each bar graph (optical density at 400 nm) represents fibril formation relative to that of WT TTR (3.6 μM) assigned as 100%. Hence, 5% fibril formation equals 95% inhibition.

Diflunisal (**1**) and 4′-hydroxy-4-biphenylcarboxylic acid (**2**) were esterified with trimethylsilyldiazomethane in CH_2Cl_2 in preparation for the coupling reactions (Scheme 1). The methyl ester of **3**, compound **9**, was prepared from a palladium-catalyzed coupling of 4-benzyloxyaniline (**6**) and methyl 2-bromobenzoate (**7**) followed by liberation of the phenol by hydrogenolysis of the benzyl ether **8**. The phenols **4**, **5**, and **9** were then reacted with cesium carbonate and various dihaloalkanes in DMF or coupled to diols (some with internal alkenes and alkynes) via a Mitsunobu reaction. The heterobivalent

(17) Schneider, F.; Hammarstrom, P.; Kelly, J. W. *Protein Sci.* **2001**, *10*, 1606−1613.
(18) Purkey, H. E.; Dorrell, M. I.; Kelly, J. W. *Proc. Natl. Acad. Sci. U.S.A.* **2001**, *98*, 5566−5571.
(19) Hammarstrom, P.; Jiang, X.; Kelly, J. W. *Proc. Natl. Acad. Sci. U.S.A.* **2002**, *99*, 16427−16432.

Scheme 1. Synthesis of Methyl Esters **4**, **5**, and **9**

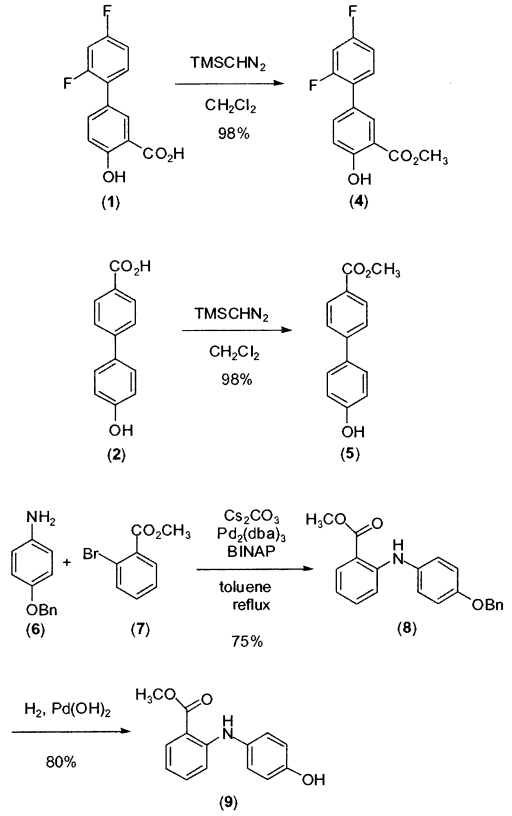

Scheme 2. Synthesis of Heterobivalent Inhibitors **20**−**29**

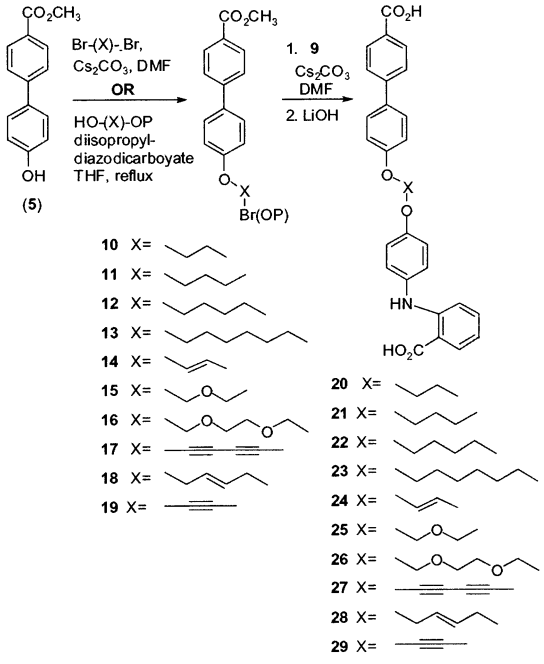

compounds were synthesized in a stepwise manner (Scheme 2), while the homobivalent inhibitors were afforded in a single pot (Scheme 3). Hydrolysis of the diesters to the diacids was accomplished with LiOH.

Fibril Formation Assays. All of the bivalent inhibitors prepared in this study, with the exception of the more hydrophilic molecules **26** and **36**, were poor inhibitors in the standard TTR fibril formation assay. In this evaluation, tetrameric TTR (3.6 μM) was preincubated with a potential inhibitor (7.2 μM)

Scheme 3. Synthesis of Homobivalent Inhibitors **30**−**43**

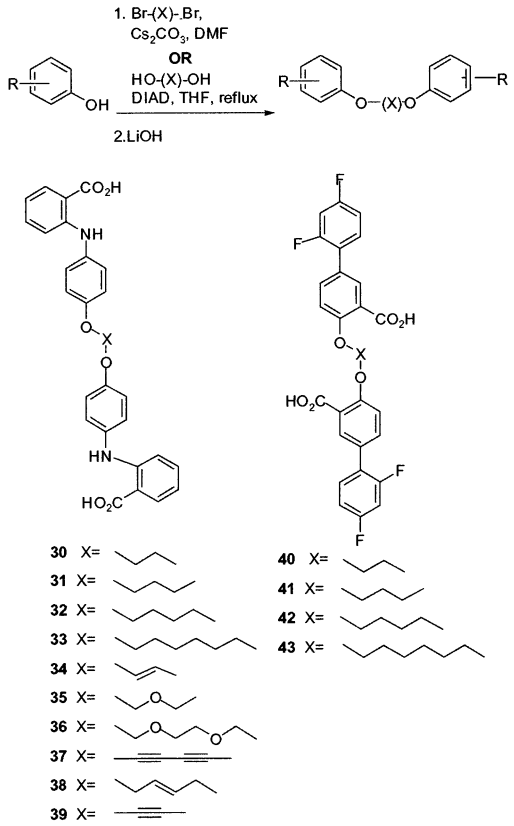

under physiological conditions for 30 min at pH 7.4. After the preincubation period, TTR was acidified to pH 4.4 and incubated at 37 °C for 72 h, the time required for WT TTR to exhibit a maximum in fibril formation as judged by turbidity at 400 nm. Fibril formation is reported relative to that of WT TTR in the absence of inhibitor—assigned to be 100%. Hence, 5% fibril formation in the presence of a given inhibitor corresponds to 95% inhibition. The monovalent inhibitors **1**, **2**, and **3** (Figure 3, inset) were highly efficacious at a concentration of 7.2 μM (Figure 3, green bars), whereas all of the bivalent inhibitors evaluated by the standard assay at this concentration gave poor inhibition (Figure 3, blue bars).[4a] **26** and **36** are effective inhibitors in the traditional acid-mediated assay, yet they do not perform as well as **2** and **3**. These inhibitors do not appear to function in the bivalent binding mode since their performance in the methanol assay is poor relative to that of the TTR·**26** and TTR·**36** complexes formed by reconstitution (Supporting Information, Figure 1).

Pre- or Coassembly-Mediated Binding of the Bivalent Inhibitors to TTR and Fibril Inhibition. Since acid-mediated fibril formation was not substantially inhibited even upon extended preincubation of folded TTR with the bivalent inhibitors (except **26** and **36**) under physiological conditions (relative to **1** and **3**), it was assumed that binding via the threading mechanism and the subunit exchange mechanism was inefficient, if even possible. With the exception of **26** and **36**, these inhibitors appear unable to bind to TTR with significant affinity in a monovalent mode, which necessitates an orientation opposite to that preferred.[9,10] To discern whether the bivalent inhibitors could intercept TTR after folding but before assembly into a tetramer, WT TTR was dissociated and unfolded at pH 2.0 for 72 h. Bivalent inhibitors (10 equiv) were added to the

unfolded protein, after which refolding and assembly was initiated by rapid dilution and neutralization of the pH. Concentration and gel filtration chromatography removed the excess small molecule remaining after TTR reconstitution. Figure 3 (red bars) demonstrates that bivalent inhibitors **20**, **22**, **25**−**28**, **36**, and **37** loaded into TTR by the pre- or coassembly mechanism dramatically inhibited TTR amyloidosis (11%, 6%, 12%, 9%, 11%, 19%, 22%, and 17%, respectively) at pH 4.4, at an inhibitor stoichiometry of 1, discerned by HPLC analysis (see below). The homobivalent inhibitors were generally not as active as the heterobivalent inhibitors derived from 4′-hydroxy-4-biphenylcarboxylic acid and anthranilic acid substructures, Figure 3.

The A25T TTR variant associated with CNS amyloidosis exists as an unstable tetramer that dissociates 1200-fold faster than the wild type. Under acid-mediated (pH 5.0) amyloidosis conditions, A25T TTR forms fibrils much more quickly (complete within 1 h) than wild-type TTR, in keeping with the fact that tetramer dissociation is the rate-limiting step of amyloidogenesis. The refolded A25T·**22** complex, however, requires 8.5 h to reach that level of fibril production, suggesting significant tetramer stabilization.

Determination of Bivalent Inhibitor Binding Stoichiometry. Reverse-phase HPLC analysis of a given TTR·bivalent inhibitor complex provides the number of molar equivalents of inhibitor bound to each TTR tetramer. TTR dissociation was accomplished by incubating the complex in acetonitrile containing 0.05% trifluoroacetic acid for several minutes, liberating the inhibitor. This preparation was then injected onto a reverse-phase column. The resulting TTR and small-molecule peaks were integrated and compared to calibration curves for the integrated area per mole of each species. Each of the bivalent inhibitors exhibiting efficacy (**20**−**43**) exhibited a binding stoichiometry of 1 mol (±15%) of compound/mol of TTR. In addition, velocity analytical ultracentrifuge experiments showed that the TTR·**22** complex exists as a tetramer (>95%) at room temperature in 10 mM phosphate buffer (pH 7.6).

X-ray Cocrystal Structures of the WT TTR·22 and WT TTR·20 Complexes. The three-dimensional structures of WT TTR·**20** and WT TTR·**22** (Figures 4A and 5) have been determined by high-resolution X-ray crystallography and refined to a crystallographic *R*-factor of 21.0% (*R*-free is 22.4%) and 20.5% (*R*-free is 23.3%), respectively (Table 1). In both TTR·bivalent inhibitor complexes, clear electron density was observed for a single inhibitor molecule spanning both thyroxine sites of a tetramer. In both cases, electron density was observed that unambiguously defines the orientation of the biphenyl and biphenylamine substructures in the T4 binding sites and defines the linker in the narrow channel connecting the two binding sites. Both **20** and **22** bind to WT TTR in a similar fashion and form comparable interactions. Both binding sites of a TTR tetramer are generally thought to be identical; hence, it was surprising that we observed asymmetric binding in the crystal structure. In both bivalent inhibitor bound structures, the BD dimer (Figure 1; preferring the biphenyl substructure in this T4 site) shows significant conformational variation from the AC dimer (the biphenylamine substructure prefers this T4 site; Figure 1), Figure 4B, yellow and green. Interestingly, there is very little conformational deviation between the BD dimers of **20** and **22** (Figure 4B, light green and dark green). Similarly,

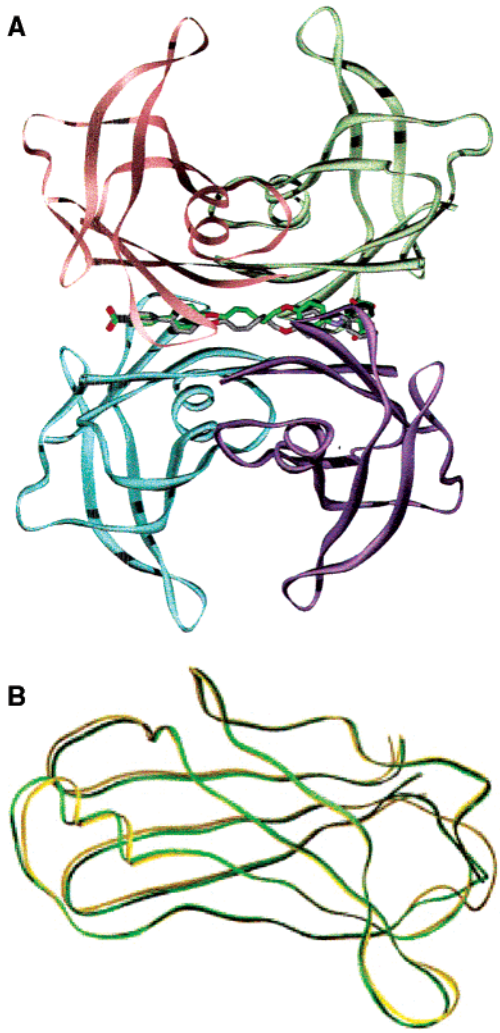

Figure 4. (A, top) Ribbon diagram representation of the X-ray cocrystal structure of the WT TTR·**22** complex**.** The two symmetry-equivalent binding modes of **22** are shown by the predominantly gray and green molecules binding to both thyroxine sites simultaneously. (B, bottom) Overlay of the A (green) and B (yellow) subunit folds from the crystal structures of WT·**20** and WT·**22** demonstrating that subunit folds in the AC and BD dimers are slightly different (Figure 1). The BD dimer, preferring biaryl substructures, has the same 3D fold in **20** (light green) and **22** (dark green). The AC dimer, preferring biarylamine substructures, has the same 3D fold in **22** (light yellow) and **20** (dark yellow). The identical subunit folds of the AC dimer are distinct from the identical subunit folds of the BD dimer.

the AC dimer of **20** is close to that of **22** (Figure 4B, light and dark yellow). Either the T4 binding site recognition substructures in the asymmetric inhibitors show a specific preference toward either the AC or BD binding pockets or the binding of the asymmetric bivalent inhibitor induces a conformational change that optimizes the protein to bind distinct substructures. In both **20** and **22**, the short helical region located between the EF sheets of the AC dimer shows a significant deviation from the previously reported apo and complexed structures of TTR.

Binding of 20 and 22 to TTR. The X-ray structure of WT TTR·**20** (Figure 5A) shows that the bivalent inhibitor complements the molecular surface of the two T4 binding sites and the intervening narrow channel very nicely. Because the crystallographic 2-fold axis bisects both T4 binding sites and the narrow channel, the bivalent inhibitor binds to TTR in two binding modes with equal occupancy which are interconverted by a C_2 rotation (*z*-axis). The ligand protein interactions are

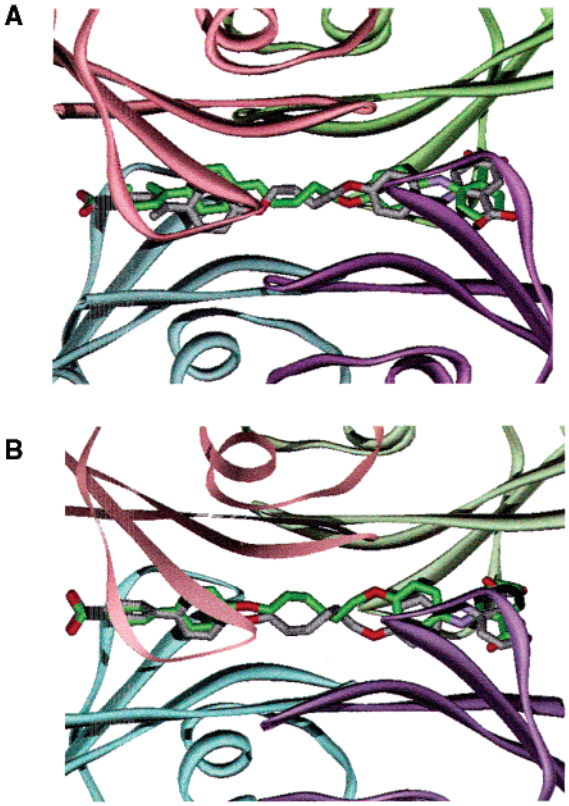

Figure 5. (A, top) Close-up ribbon depiction of the WT TTR·**20** cocrystal structure. The two symmetry-equivalent binding modes are shown by the structures colored predominantly in green and gray. (B, bottom) Close-up ribbon depiction of the WT TTR·**22** cocrystal structure. The two symmetry-equivalent binding modes are shown by the structures colored predominantly in green and gray.

Table 1. Structural Parameters for the WT·**20** and WT·**22** X-ray Cocrystal Structure

	TTR·**22**	TTR·**20**
unit cell params (Å)	42.78, 84.61, 65.73	42.59, 84.35, 65.57
resolution (Å)	22.19−1.65	42.26−1.46
no. of unique reflns	29034	38794
completeness (%) (overall/outer shell)	98.3/96.6	97.3/94.0
R_{sym} (overall/outer shell)	0.05/0.33	0.05/0.44
	Refinement Statistics	
resolution (Å)	22.19−1.65	42.18−1.50
R-factor/*R*-free (%)	20.5/23.3	21.0/22.4
rmsd bond length (Å)	0.05	0.04
rmsd bond angle (deg)	2.1	2.5

dominated by nonpolar contacts. Both the biphenyl and biphenylamine moieties are stacked between the hydrophobic side chains of Leu 17, Leu 17′, Ala 108, Ala 108′, Leu 110, Leu 110′, Thr 119, and Thr 119′ in the AC and BD binding pockets, respectively (Figure 5A). These interactions stabilize the tetrameric form of TTR through a series of van der Waals and hydrophobic interactions. Hydrogen bonding also contributes to the molecular interactions observed in both T4 binding pockets. Specifically, the carboxyl group of the biphenyl moiety in both binding modes makes a strong hydrogen bond with the Lys 15 or Lys 15′ comprising the outer binding pocket of the BD dimer. Deep within the binding pockets of AC and BD, the ether oxygens of the biphenylamine and biphenyl moieties make hydrogen bonds with residues Ser 117 and Ser 117′ of the TTR tetramer. In fact, Ser 117, Ser 117′, Thr 119, and Thr 119′

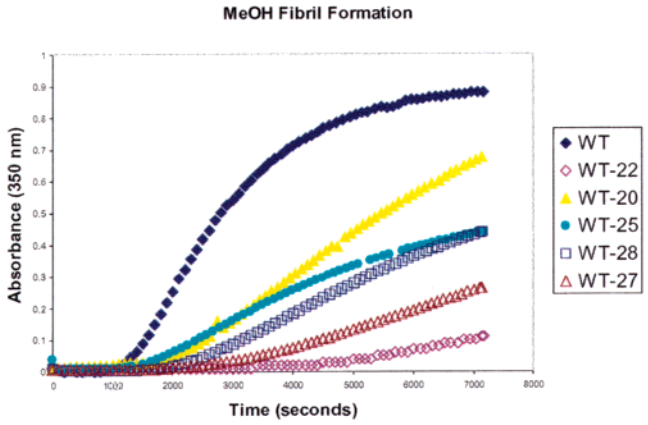

Figure 6. MeOH-mediated (50%) fibril formation time course of WT, WT TTR·**20**, WT TTR·**22**, WT TTR·**25**, WT TTR·**27**, and WT TTR·**28** complexes. The turbidity at 350 nm is plotted as a function of time (s). The best inhibitors (**22** and **27**) are the best observed to date in this medium.

residues adopt multiple conformations to facilitate additional electrostatic and hydrophobic interactions with the neighboring residues dependent on the conformation of the bivalent inhibitor. In the outer binding pocket of the AC dimer, the *o*-carboxyl substituent of the biphenylamine makes a water-mediated electrostatic interaction with residues Lys 15, Lys 15′, Glu 54, and Glu 54′. The intramolecular hydrogen bond between the *o*-carboxyl group and *p*-amino group of the inhibitor also stabilizes the biphenylamine moiety in the BD binding pocket. The distance between the two ether oxygen groups is 5.2 Å, and the four methylene units of the linker are primarily stabilized by hydrophobic interactions with the Cβ atoms of all four Ser 117 residues of the TTR tetramer.

The X-ray structure of the WT TTR·**22** complex shows that the inhibitor also complements the hormone binding channel with interactions very similar to those described above for the TTR·**20** complex structure (Figure 5B). Both biphenyl and the biphenylamine moieties were slightly displaced toward the outer binding pocket to accommodate the linker composed of six methylene groups. The distance between the two ether oxygen groups is 7.8 Å, and the methylene groups of the linker chain are again stabilized by interactions with the Cβ atoms of Ser 117. The Ser 117 residue in the AC dimer adopts a different orientation compared to **20** to form a hydrogen bond with the ether oxygen of the biphenyl moiety. Thr 119 of the AC dimer is also slightly shifted toward the biphenyl substructure in **22** compared to **20**.

Inhibiting Amyloidosis Mediated by Organic Solvent Treatment. The rate of WT TTR fibril formation is dramatically increased when amyloidosis is mediated by 50% methanol treatment, reaching completion in 2 h as opposed to 72 h in acid-facilitated amyloidogenesis. Hence, methanol-mediated amyloidogenesis is a stringent test of inhibitor efficacy. Many of our monovalent inhibitors are far less effective in an aqueous methanol denaturing environment compared to an acid denaturing environment. In contrast, when the WT TTR·**22** complex was subjected to amyloid formation in 50% methanol, amyloidosis was reduced to 10% over a 2 h period, Figure 6. Inhibitor **27** is nearly as good, whereas inhibitors **20**, **25**, and **28** are not as potent as **22** in this denaturing environment.

Probing Mechanism: Evaluating WT TTR·20, WT TTR·22, and WT TTR·25 Tetramer Dissociation in Urea. Previ-

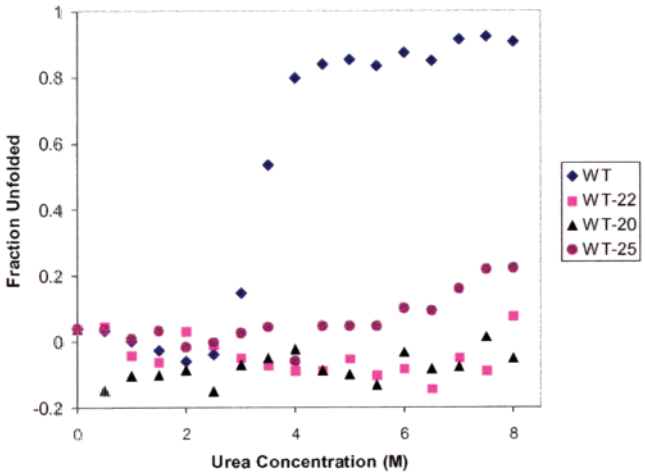

Figure 7. Urea denaturation curves for WT TTR and the WT TTR·**20**, WT TTR·**22**, and WT TTR·**25** complexes. TTR (0.1 mg/mL) or TTR· inhibitor complexes were incubated as a function of urea concentration at room temperature (120 h). The far-UV CD ellipticity at 214−218 nm was compared to that of WT to determine the fraction of TTR that was unfolded at each concentration. The C_M of unfolding for WT TTR is 3.5 M. The WT TTR·**20**, WT TTR·**22**, and WT TTR·**25** complexes do not appreciably denature in urea.

ously, we have studied the rate of tetramer dissociation in the absence and presence of monovalent inhibitors by linking tetramer dissociation (slow step) to fast unfolding in urea concentrations in the post unfolding transition region of the urea denaturation curve.[11,19] To establish that post transition urea concentrations are employed, urea denaturation curves of WT TTR as well as WT TTR·**20**, WT TTR·**22**, and WT TTR·**25** were recorded employing far-UV CD spectroscopy to monitor unfolding. Wild-type TTR exhibits a C_m at 3.4 M urea as demonstrated previously.[19] In contrast the bivalent inhibitor bound complexes exhibit no significant denaturation, even when incubated in 8.0 M urea solutions for 120 h, Figure 7. These results imply that the bivalent inhibitor·TTR complexes exhibit kinetic stabilization toward urea denaturation. Apparently binding of the bivalent inhibitor to the ground state lowers its free energy and increases the dissociative activation barrier so much that it is not surmountable in concentrated urea solutions.

Measuring the Apparent Dissociation Rate of Inhibitor 22 from the TTR·22 Complex. The apparent bivalent inhibitor dissociation rate was evaluated by capturing the WT TTR·**22** complex using a Sepharose-conjugated anti-TTR polyclonal antibody. The antibody-captured WT TTR·**22** complex was subjected to sixteen 10 min washes with TSA (10 mM Tris−HCl, pH 8.0, 140 mM NaCl, 0.025% NaN_3) buffer.[18] Since the inhibitor cannot bind folded TTR tetramers (Figure 3), we were not concerned about rebinding after dissociation; hence, these experiments are equivalent to flow washing experiments used earlier for this purpose.[18] The amount of ligand lost after each wash was determined by the HPLC method previously described.[18] There was no statistically significant loss of **22** from the TTR·**22** complex after 160 min of gentle rocking in buffer, Figure 8.

Templating D18G Tetramer Formation with Bivalent TTR Binders. D18G is a highly destabilized transthyretin variant whose secretion into the CSF leads to misfolding and deposition on the leptomenigial membrane, resulting in CNS pathology.[7c] D18G exists primarily as a monomer under physiological conditions and readily aggregates under mild

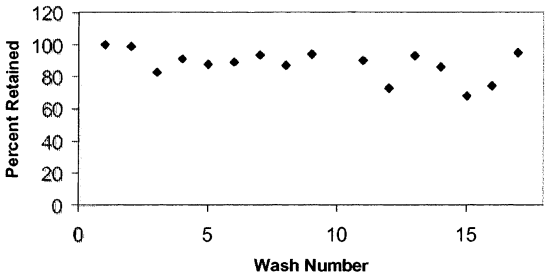

Figure 8. Inhibitor **22** dissociation rate from WT TTR evaluated by capturing the WT TTR·**22** complex with an anti-TTR antibody immobilized on a Sepharose resin. The percent of ligand retained based on RP-HPLC analysis was determined after each of sixteen 10 min washes.

denaturing conditions (pH 5.0, 37 °C) and slowly under physiological conditions.[7c] The bivalent molecules studied herein (14.4 μM) were incubated with freshly purified D18G monomers (14.4 μM monomer, 3.6 μM if it were a tetramer) at room temperature for 18 h (pH 7). The ability of the bivalent inhibitors to induce tetramer formation was evaluated by glutaraldehyde cross-linking followed by SDS−PAGE analysis, Figure 9a−c. In the absence of inhibitor, D18G forms soluble aggregates that remain at the top of the gel (in the stacking gel). Most of the inhibitors were efficient at forming D18G tetramers at 25 °C. A 72 h incubation of D18G with **22** did not diminish the extent of tetramer formation, indicating that these tetramers are quite stable under these conditions and not prone to aggregation (25 °C, Supporting Information, Figure 2). When the incubation was performed at 37 °C, however, most of the bivalent inhibitors were unable to compete with the increased efficiency of monomer aggregation and much less tetramerization resulted (Figure 9d−f). Only inhibitors **36** and **37** were effective at tetramer stabilization and preventing thermal aggregation.

Discussion

The affinity of bivalent ligand binding to a receptor with two sites is sometimes higher than the summation of the individual contributions. This increased binding affinity is not necessarily a result of "positive cooperativity", since the individual interaction(s) involved may have either a positive or a negative effect on the binding free energy of the other molecular recognition event. Instead of cooperativity, Whitesides et al. propose the use of the enhancement parameter β to describe the enhanced affinity of polyvalent interactions.[12] In this case, β is equal to the ratio of the association constant of the bivalent interaction to the affinity of the monovalent equivalent. A large value for β indicates a beneficial polyvalent interaction, and is even possible when the ligand binds with negative cooperativity. Unfortunately, we were unable to measure an affinity constant for the bivalent inhibitors described here because inhibitor binding is linked to TTR reassembly which appears irreversible on the basis of the exceedingly slow rate of inhibitor dissociation and the inability of the TTR·bivalent inhibitor complex to dissociate, even in strong denaturants.

Maximizing β involves making the linker as rigid as possible to minimize the conformational entropy penalty associated with bivalent binding without introducing strain and diminishing the enthalpy of binding. An ideally designed rigid bivalent inhibitor will only have to pay the translational and rotational entropy penalty associated with binding once. As long as the conformational entropy penalty is smaller than the translational and

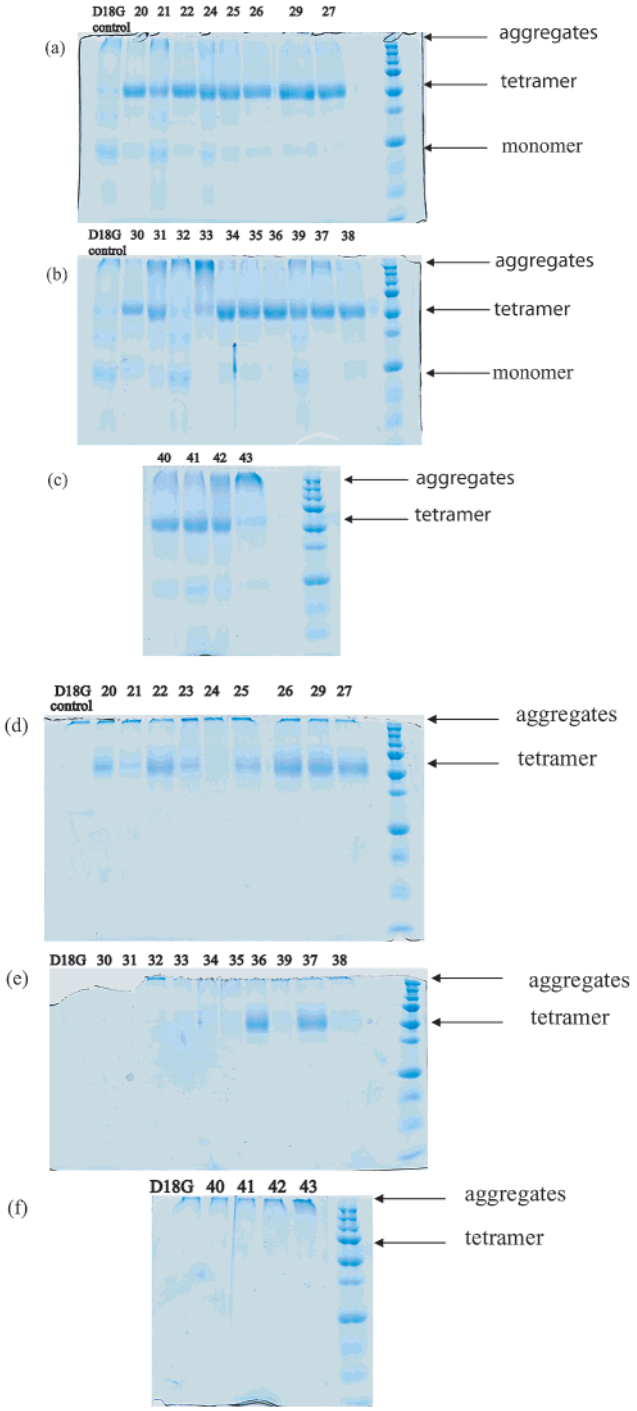

Figure 9. Efficacy of bivalent inhibitor mediated tetramerization of D18G TTR. Inhibitors were incubated with freshly purified monomeric D18G TTR for 18 h before glutaraldehyde cross-linking and SDS−PAGE analysis. (a) Data from inhibitors **20**−**29** (25 °C). **(**b**)** Data from inhibitors **30**−**39** with D18G monomers (25 °C). (c) Data from inhibitors **40**−**43** (25 °C). (d) Data from inhibitors **20**−**29** (37 °C). (e) Data from inhibitors **30**−**39** (37 °C). (f) Data from inhibitors **40**−**43** (37 °C).

rotational entropy penalty and the enthalpy of binding at both sites is substantial, a large β will be observed. Bivalent inhibitors typically prefer to bind in a monovalent fashion when the conformational energy penalty exceeds the ΔS for translation and rotation. This is less of a concern here because monovalent binding requires that the substructure occupying the T4 binding site in an orientation opposite that preferred. In many cases this preference is substantial. Hence, we can maximize the enthalpy of binding by building some conformational flexibility into the linker to compensate for design imperfections without getting predominant monovalent binding.

Analysis of several transthyretin·monovalent inhibitor cocrystal structures reveals that the channel connecting the C_2-symmetric inner binding sites is quite narrow.[9] Therefore, a properly designed linker could contribute to the binding energy, provided the linker complements the surface of the channel. We focused on identifying linkers of the appropriate length and rigidity that were as sterically unencumbered as possible. Alkyl, alkenyl, alkynyl, and ethylene glycol linkers were chosen on the basis of these criteria. We chose T4 binding site substructures that bind TTR with high affinity and exhibit impressive in vitro fibril formation inhibition at a concentration of 7.2 μM (3.6 μM TTR). This list was further narrowed to those bearing phenol substituents that enable covalent linkage of binary combinations of these substructures. Monovalent inhibitors meeting these criteria include diflunisal (**1**), which reduces fibril formation to 4% of that of a WT control, and 4′-hydroxy-4-biphenylcarboxylic acid (**2**) and 2-(4-hydroxyphenylamino)benzoic acid (**3**), which exhibit 7% and 10% fibril formation, respectively.

The bivalent inhibitors studied herein were generally unable to prevent wild-type TTR fibril formation when incubated with the protein in its native tetrameric structure, implying that the majority of the bivalent inhibitors could not bind by a threading mechanism or subunit exchange, with the possible exception of **26** and **36**. It was necessary to refold and reassemble denatured TTR around the inhibitor to enable bivalent inhibitor binding. Most of the inhibitor·TTR complexes formed by the pre- or coassembly mechanism exhibited vastly improved fibril inhibition profiles (Figure 3). At a stoichiometry of 1 equiv of compound **22** per TTR tetramer, only 6% of WT TTR fibril formation is observed, while **20** and **25**−**27** all reduce acid-mediated amyloidogenesis to ∼10% of that of a WT control. These are the best inhibitors at this stoichiometry discovered by our laboratory to date. Strong evidence for the 1:1 stoichiometry of **20** and **22** relative to TTR derives from X-ray cocrystal structures, wherein it is possible to observe the electron density of the linker in the central channel and the expected orientation of the substructures within the T4 binding sites. Quantitative HPLC analysis also revealed a stoichiometry of 1:1.

It has been suggested that the binding of thyroxine in one binding pocket confers rigidity on the second binding site, resulting in negatively cooperative binding which characterizes the binding of most ligands to the second site.[13] Some of the monovalent inhibitor·TTR structures reveal dissimilarity between the two hormone binding pockets.[20,21] The TTR·monovalent inhibitor complexes display better electron density for the substructure in the BD dimer when compared to that in the AC dimer. The differences between the bound AC and BD dimers suggest that the biphenyl and biphenylamine substructures of a heterobivalent inhibitor may show a preference for one binding pocket over the other. Indeed, the BD binding pocket exhibits a binding preference for biphenyls. The heterobivalent compounds **20**−**29** gave better activity than their

(20) Adamski-Werner, S. L.; Kumar, P. S.; Sacchettinni, J. C.; Kelly, J. W. *J. Med. Chem.*, in press.
(21) Ghosh, M.; Meerts, I. A. T. M.; Cook, A.; Bergman, A.; Brouwer, A.; Johnson, L. N. *Acta Crystallogr.* **2000**, *D56*, 1085−1095.

symmetric analogues, consistent with the idea that the two binding pockets are slightly different; hence, a molecule with two different T4 binding substructures could result in optimal binding to the two slightly different sites.

The length of the linker appears to be very important in the heterobivalent inhibitors, with butyl and hexyl being superior to pentyl and octyl. An analysis of the cocrystal structure of **22** bound to TTR reveals that the hexyl chain is kinked, not adopting the expected extended all-*anti* conformation. From the disrupted electron density of the inhibitor in the channel of the crystal structure, it is likely that the linker may exist in more than one nonextended conformation. The oxygen to oxygen distance in the linker is approximately 0.9 Å shorter than that in an all-*anti* conformation. Interestingly, the butyl chain also deviates from the expected extended conformation, being 0.5 Å shorter (Figure 5A). This compact conformation of the butyl group requires the substructures to bind deeper into the inner binding pocket in comparison to those of **22**. The octane linker appears to be too long to be accommodated in either an extended or a kinked conformation. Both of the ethylene glycol linkers appear to complement the binding channel, possibly owing to their propensity to adopt *gauche* conformations. The introduction of more rigid dialkyne and hexene linkers affords very good inhibitors; however, the monoalkyne and the butene linkers are not optimal.

The anthranilic acid based homodimers **30**−**39** exhibit a different trend in terms of the preferred linkers for optimal amyloid inhibition. The hexadiyne linker is favored; however, its activity is only 6% better than that of the saturated hexyl linker (17% and 24%, respectively). The second best linker is triethylene glycol. Incorporation of unsaturation into the butyl linker (alkene **34** or alkyne **39)** resulted in a loss of activity. Introduction of one unit of unsaturation into the hexyl linker (**38**) resulted in a modest inhibitor (40% fibril formation).

Interestingly, the length of the chain in the homodimers based on diflunisal (**40**−**43**) does not appear to make a difference in the limited group prepared. All four molecules allow the same extent of fibril formation (about 40%). The crystal structure of diflunisal bound to transthyretin has recently been determined.[20] The fluorinated ring can bind in the inner or outer halogen binding pocket with little preference for one over the other. These molecules may prefer to bind in the opposite sense from the orientation required for binding in a bivalent sense; hence, we stopped making analogues in this series.

The Wild-Type TTR·20, TTR·22, and TTR·25 Complexes Do Not Dissociate. One notable feature of the TTR·bivalent inhibitor complexes is that the tetramer does not dissociate, even in highly denaturing environments. In addition, the bivalent inhibitor does not dissociate from the tetramer. The physiological trigger for amyloidogenesis in vivo is not currently understood, nor has the denaturing environment been identified. Therefore, we find it prudent to test our inhibitors under a variety of denaturing stresses to ensure selection of the best molecule. Three different denaturation environments allow scrutiny of the compounds including acid-mediated fibril formation (pH 4.4 for the WT, pH 5.0 for A25T), organic-solvent-mediated fibril formation (50% methanol), and urea denaturation of the TTR tetramer. The three best wild-type complexes, WT TTR·**20**, TTR·**22**, and TTR·**25**, perform well under all three denaturation stressses.

Bivalent Inhibitors and CNS Amyloidosis. The majority of transthyretin disease-associated mutations do not result in central nervous system pathology. D18G and A25T, however, are representatives of a growing group of TTR variants that are characterized by deposition in the leptomenigal vessels and in the subarachnoid membrane that leads to CNS dysfunction. The high concentration of thyroxine in the choroid plexus is believed to chaperone small amounts of the CNS-associated TTR variants into the CSF where T4 dissociation enables TTR dissociation, resulting in fibril formation owing to thyroxine's low affinity. Small molecules that bind with very high affinity and maintain transthyretin's tetrameric structure in the CSF should be useful for preventing CNS amyloidosis. A bivalent inhibitor could be ideal for this application owing to the kinetic stability of the inhibitor·TTR complex. A bivalent inhibitor that crossed the blood−brain barrier and dramatically stabilized D18G or A25T could be therapeutically useful.

All of the bivalent inhibitors were evaluated for their ability to template D18G tetramer formation, employing freshly purified D18G TTR. D18G TTR is largely a monomeric protein found in very low concentrations in the plasma and CSF of individuals of Hungarian descent with CNS pathology. This remarkably unstable variant is prone to extensive aggregation even under physiological conditions. Previous work from our laboratory demonstrates that the D18G tetramer is destabilized by ∼10 kcal/mol relative to wild-type TTR.

Several bivalent inhibitors prevented the aggregation of D18G for 24 h through native-state stabilization. When the experiment was repeated at 37 °C (where aggregation is more efficient), fewer compounds were efficacious. Although we have yet to find the perfect molecule, we have shown that it is possible to stabilize D18G with bivalent molecules under physiologically relevant conditions.

Whereas D18G TTR is primarily monomeric, A25T is an unstable tetramer. Maximal acid-mediated fibril formation with A25T occurs at pH 5.0, significantly higher than the acidic maximum for the wild-type protein (pH 4.4). A25T fibril formation is complete in less than 1 h (pH 5.0), which is 72-fold faster than that of the wild type (pH 4.4). When the A25T tetramer was refolded around ligand **22**, the time required for maximum fibril formation was increased to 8.5 h. An optimized inhibitor could impart even greater native-state stabilization for the CNS TTR variants.

Conclusions

X-ray crystallography and quantitative HPLC analysis demonstrate that several inhibitors synthesized herein bind simultaneously to both thyroxine binding sites. Transthyretin can assemble around these bivalent inhibitors during reconstitution, but generally speaking, these molecules do not bind to native TTR. Cell-permeable bivalent inhibitors that get into the lumen of the endoplasmic reticulum in the liver (secretes TTR into blood) or the choroid plexus (secretes TTR into CSF) should intercept TTR via the pre- or coassembly mechanism. At a stoichiometry of 1:1, the best inhibitor reduced acid-mediated TTR amyloid fibril formation to 6% of that exhibited by WT TTR, a significant improvement over the ∼30% observed for the best monovalent inhibitors (TTR and monovalent inhibitor concentrations are both 3.6 μM). The apparent dissociation rate of the best bivalent inhibitor is effectively zero, consistent with

the idea that TTR tetramer dissociation and small-molecule inhibitor dissociation are linked.

Materials and Methods

Protein Expression and Purification. WT, A25T, and D18G TTR were expressed and purified from *E. coli* as described previously.[22] WT and A25T express as soluble homotetramers, while D18G forms inclusion bodies.

Purification of D18G from Inclusion Bodies. D18G TTR was purified from inclusion bodies by the method described previously.[7c] The total yield of pure monomeric protein was 3−5 mg/L of culture. For all D18G experiments, it is imperative to use freshly gel filtered protein.

Pre- or Coassembly-Mediated Binding of the Bivalent Inhibitors to TTR. Transthryretin solutions (10 mg, 7.6 μM (0.4 mg/mL) in 10 mM sodium phosphate buffer (pH 7.0), 100 mM KCl, 1 mM EDTA) were dialyzed against 4 L of deinonized water overnight using a 10000 MW cutoff membrane. Unfolding was accomplished by continuing to dialyze against 4 L of pH 2.0 water for 72 h at 4 °C. The protein was diluted to 1.8 μM (0.1 mg/mL, pH 2.0), and then added to an equal volume of 200 mM sodium phosphate buffer (pH 7.4) with 1 mM EDTA, and containing an 18 μM (10 equiv relative to the TTR tetramer) concentration of the desired bivalent inhibitor in DMSO. The resulting solution was mixed rapidly with a stir bar and concentrated in an Amicon concentrator using a 10000 MW cutoff membrane. The protein was purified by gel filtration using a Superdex 75 column eluting with 10 mM sodium phosphate buffer (pH 7.0) containing 100 mM KCl and 1 mM EDTA.

Determination of Inhibitor:TTR Stoichiometry by RP HPLC. Transthyretin·bivalent inhibitor solutions prepared by the pre- or coassembly mechanism (3.6 μM, 0.2 mg/mL TTR) were diluted 10-fold into acetonitrile and immediately loaded into a Waters 71P autosampler. The resulting solution was injected (135 μL) onto a Keystone 3 cm C_{18} reversed-phase column at 100% solution A. After a 3 min hold at 100% A, a 40−100% linear gradient of solution B over 8 min was utilized to elute both TTR and the bivalent inhibitor. Solution A is composed of 94.8% water, 5% acetonitrile, and 0.2% trifluoroacetic acid. Solution B contains 94.8% acetonitrile, 5% water, and 0.2% trifluoroacetic acid. Detection at 280 nm was accomplished with a Waters 486 tunable absorbance detector. The integrated peaks of the small molecule and TTR were compared to calibration curves prepared from known amounts of small molecules and TTR.

Glutaraldehyde Cross-Linking and SDS−PAGE. Freshly prepared D18G TTR samples (0.2 mg/mL, 14.4 μM monomer) were incubated in the presence of 28.8 μM bivalent inhibitors at 25 °C for 24 h. Glutaraldehyde cross-linking of the protein was performed on 50 μL aliquots of sample by adding 5 μL of glutaraldehyde (25%). The cross-linking reaction was allowed to proceed for 4 min before it was quenched by addition of 7% $NaBH_4$ (5 μL) in 0.1 M NaOH. The sample was mixed with 15 μL of SDS reducing gel loading cocktail (6×) and boiled for 5 min prior to SDS−PAGE gel electrophoresis (12%). The cross-linked protein was visualized by Gel Code staining.

TTR Urea Denaturation Curves by Circular Dichroism. TTR (0.1 mg/mL, 1.8 μM tetramer) was incubated at variable concentrations of urea in 50 mM phosphate buffer (pH 7.0) containing 100 mM KCl, 1 mM EDTA, and 1 mM DTT (1.0 mL total volume). Circular dichroism spectra were recorded after a 120 h incubation period (25 °C) using a wavelength scan from 220 to 214 nm, sampling every 0.5 nm. The signal from 218 to 215 nm was averaged and plotted to determine the fraction of TTR tetramer that was unfolded at each urea concentration.

Traditional Stagnant Transthyretin Amyloid Fibril Formation Assay. A 0.495 mL sample of TTR (7.6 μM (0.4 mg/mL) in 10 mM sodium phosphate, 100 mM KCl, and 1 mM EDTA at pH 7) was incubated with 5 μL of bivalent inhibitor in DMSO (0.76 or 1.44 mM). After 30 min, the samples were diluted with 0.5 mL of 100 mM acetate buffer (pH 4.2) containing 100 mM KCl and 1 mM EDTA. Samples were briefly vortexed and then further incubated at 37 °C for 72 h without stirring. The extent of fibril formation was probed by turbidity measurements at 350 and 400 nm on an HP 845x UV−vis spectrometer. Single-time-point samples (72 h) were vortexed immediately before the measurement.

Stagnant Amyloid Fibril Formation Assay on Preformed TTR·Bivalent Inhibitor Complexes. A 0.495 mL sample of a TTR·bivalent inhibior complex of 1:1 stiochiometry (3.6 uM) in 10 mM phosphate buffer (pH 7.0) containing 100 mM KCl and 1 mM EDTA was diluted with 0.5 mL of 100 mM acetate buffer (pH 4.2) containing 100 mM KCl and 1 mM EDTA. Samples were briefly vortexed and then further incubated at 37 °C for 72 h without stirring. The extent of fibril formation was probed by turbidity measurements at 350 and 400 nm on an HP 845x UV−vis spectrometer. Single-time-point samples (72 h) were vortexed immediately before the measurement.

TTR Fibril Formation Kinetics in 50% Methanol. TTR·bivalent inhibitor samples (214 μL, 28.5 μM (1.5 mg/mL)) in 10 mM phosphate buffer (pH 7.0) containing 100 mM KCl and 1 mM EDTA were added to a 3 mL cuvette containing 1.786 mL of methanol buffer (84% methanol, 16% water, 100 mM KCl, 1 mM EDTA, 1 mM DTT, pH 7.0) and 1.0 mL of Tris buffer (50 mM Tris−HCl, 100 mM KCl, 1 mM EDTA, 1 mM DTT, pH 7.8) with stirring at 25 °C. The turbidity was continuously monitored over 7200 s at 400 nm.

TTR Antibody Purification and Conjugation to Sepharose. Antibodies were purified by passage of rabbit serum over a recombinant staphylococcal protein A column. The column was washed with five column volumes of 50 mM sodium phosphate (pH 2.0) buffer, and the antibodies were eluted with five column volumes of 100 mM citrate buffer (pH 3.0). Each 5 mL elution fraction was neutralized with 1 mL of 1 M Tris−HCl buffer (pH 9.0). The fractions were then dialyzed against 100 mM sodium bicarbonate, pH 8.2. The concentrated protein was then coupled to cyanogen bromide activated Sepharose. The Sepharose gel was first washed in a filter funnel with 1400 mL of 1 mM HCl for 15 min. The coupling buffer (100 mM sodium bicarbonate, 500 mM NaCl, pH 8.3) and the antibody were added to the washed gel (5 mL of coupling buffer/g of gel and 35 mg of antibody/g of gel). The gel was rotated at room temperature for 1 h, followed by centrifugation at 3000 rpm for 1 min. The gel was transferred to 100 mM Tris−HCl buffer (pH 8.0) and was rotated at room temperature for 2 h. The gel was washed with 100 mM acetate buffer (pH 4.0) containing 500 mM NaCl and 100 mM Tris−HCl buffer (pH 8.0) containing 500 mM NaCl for two cycles. The gel was washed twice with TSA (10 mM Tris−HCl, 140 mM NaCl, 0.025% sodium azide, pH 8.0) and stored as a 1:1 slurry in TSA.

Sepharose Wash Data. A 1:1 Sepharose gel/TSA (10 mM Tris−HCl, pH 8.0, 140 mM NaCl, 0.025% NaN_3) slurry (187 μL) of quenched Sepharose (prepared by coupling 200 mM Tris−HCl (pH 8.0) to the gel instead of the antibody) was added to six 2 mL Eppendorf tubes containing 1.5 mL of TTR·bivalent inhibitor complex (3.6 μM). The mixture was incubated with agitation on a rocker at 18 rpm for 1 h (25 °C). The solution was centrifuged (14000 rpm for 1 min) and the supernatant divided into 20 aliquots of 400 μL each. A 1:1 Sepharose gel/TSA slurry of anti-TTR antibody-conjugated Sepharose (200 μL) was added to each aliquot, and the resulting samples were allowed to rock at 18 rpm (4 °C) for 30 min. The samples were centrifuged (14000 rpm for 1 min), and the supernatant was removed. In each sample, the gel was washed with 1 mL of TSA/0.5% saponin at 4 °C for 10 min. The sample was centrifuged (14000 rpm for 1 min) and the supernatant removed. This wash was repeated two more times. The remaining 15 washes were performed with 1 mL of TSA. After each wash, one sample was set aside to evaluate the stoichiometry of the bivalent inhibitor by RP HPLC to detect wash-associated ligand loss. TTR·

(22) Lashuel, H. A.; Wurth, C.; Woo, L.; Kelly, J. W. *Biochemistry* **1999**, *38*, 13560−13573.

bivalent inhibitor complexes were liberated from the Sepharose-conjugated antibody by addition of 135 μL of 100 mM triethylamine (pH 11.5) during gentle rocking at 4 °C for 30 min. The samples were centrifuged, and the supernatant was analyzed using the HPLC method described above for stoichiometry determinations.

Crystallization and X-ray Data Collection. Crystals of WT TTR·**20** and WT TTR·**22** complexes were obtained from TTR·bivalent inhibitor complexes of 1:1 stoichiometry resulting from coassembly at 5−7 mg/mL (95−133 μM in 100 mM KCl, 1 mM EDTA, 10 mM sodium phosphate, pH 7.0, 0.35−0.50 M ammonium sulfate equilibrated against 2 M ammonium sulfate in hanging drop experiments). A DIP2030 imaging plate system (MAC Science, Yokohama, Japan) coupled to an RU200 rotating anode X-ray generator was used for data collection of WT TTR·**22**. The CCD detector at the monochromatic high-energy source of 19-BM-SBC3, BIOCARS, Advance Photon Source, was used for the data collection of WT TTR·**20**. The crystals were placed in paratone oil as a cryoprotectant and cooled (to 120 K for WT TTR·**22** and 100 K for WT TTR·**20**) for diffraction experiments. Crystals of TTR·ligand complex structures are isomorphous with the apo crystal form with unit cell dimensions close to $a = 43$ Å, $b = 85$ Å, and $c = 66$ Å, space group $P2_12_12$ with two monomers in the asymmetric unit. Data were reduced with DENZO and SCALEPAC.[23]

Structure Determination and Refinement. The protein atomic coordinates for apo-TTR from the Protein Data Bank (accession number 1BMZ) were used as a starting model during the molecular replacement search by EPMR.[24] The best solutions from EPMR were refined by molecular dynamics and energy minimization protocols of the CNS.[25] The resulting difference Fourier maps of WT TTR·**22** and WT TTR·**20** revealed binding of the single bivalent ligand occupying both the binding pockets of the TTR tetramer. Difference Fourier maps showed distinct and clear electron densities for both the biphenyl and biphenylamine moieties. However, continuous electron density for the linker carbons between the two binding cavities was only visible when the electron density maps were contoured below 1σ, presumably due to flexibility in that region. Despite the weak linker density, the ligand could be unambiguously placed because of the clear biphenyl and biphenylamine electron densities and was included in the crystallographic refinement. Using these maps, the ligand could be unambiguously placed into the density and was included in the crystallographic refinement. Because the 2-fold crystallographic symmetry axis bisects the binding channel (*z*-axis, Figure 1), a statistical disorder model had to be applied, giving rise to two ligand binding modes per tetrameric TTR. After several cycles of simulated annealing and subsequent positional and temperature factor refinement, water molecules were placed into difference Fourier maps. The final cycle of map fitting was done using the unbiased weighted electron density map calculated by the shake/warp bias removal protocol.[26] Both the symmetry-related binding conformations of the ligand were in good agreement with unbiased annealed omit maps as well as the shake/warp unbiased weighted maps phased in the absence of the inhibitor. The final cycle of refinement was carried out by the maximum likelihood method using CCP4-Refmac. Because of the lack of interpretable electron densities in the final map, the nine N-terminal and three C-terminal residues were not included in the final model. A summary of the crystallographic analysis is presented in Table 1.

Acknowledgment. We thank the NIH (Grant DK46335), The Skaggs Institute for Chemical Biology, and the Lita Annenberg Hazen Foundation for financial support as well as the NIH (Grant NRSA DK060304-03) for a postdoctoral fellowship (N.S.G.). Additional support was provided by the Robert A. Welch Foundation (J.C.S.). Use of the Argonne National Laboratory Structural Biology Center beam lines at the Advanced Photon Source was supported by the United States Department of Energy, Office of Energy Research, under Contract W-31-109-ENG-38. We also thank Jennifer Kowalski and Prakash Raman for their initial efforts focused on the preparation of bivalent transthyretin amyloid inhibitors, Per Hammarstrom and R. Luke Wiseman for many helpful discussions, and Songpon Deechongkit for help with analytical ultracentrifugation.

Supporting Information Available: Detailed synthesis and characterization of compounds **4**, **5**, and **8**−**43**, purification of D18G TTR from inclusion bodies, the efficiency of bivalent inhibitors for D18G tetramerization as revealed by cross-linking data for compound **22** after a 72 h incubation period, and methanol-mediated fibril formation of WT TTR preincubated with **26** and **36** and WT TTR·**26** formed by co-assembly. This material is available free of charge via the Internet at http://pubs.acs.org.

JA030294Z

(23) Otwinowski, Z.; Minor, W. *Macromolecular Crystallography*; Carter, C. W., Jr., Sweet, R. M., Eds.; Methods in Enzymology, Vol. 276, Part A; Academic Press: New York, 1997; pp 307−326.
(24) Kissinger, C. R.; Gehlhaar, D. K.; Fogel, D. B. *Acta Crystallogr.* **1999**, *D55*, 484−491.
(25) Brunger, A. T.; Adams, P. D.; Clore, G. M.; DeLano, W. L.; Gros, P.; Grosse-Kunstleve, R. W.; Jiang, J.-S.; Kuszewski, J.; Nilges, N.; Pannu, N. S.; Read, R. J.; Rice, L. M.; Simonson, T.; Warren, G. L. *Acta Crystallogr.* **1998**, *D54*, 905−921.
(26) (a) Collaborative Computational Project, Number 4. *Acta Crystallogr.* **1994**, *D50*, 760−763. (b) Murshudov, G. N.; Vagin, A. A.; Dodson, E. J. *Acta Crystallogr.* **1997**, *D53*, 240−255. (c) Kantardjieff, K.; Höchtl, P.; Segelke, B.; Tao, F.-M.; Rupp, B. *Acta Crystallogr.* **2002**, *D58*, 735−743.